Chemical Engineering Science 189 (2018) 422–430

Contents lists available at ScienceDirect

Chemical Engineering Science

journal homepage: www.elsevier.com/locate/ces

Continuous flow synthesis of ultrasmall gold nanoparticles in a microreactor using trisodium citrate and their SERS performance

He Huang [a], Hendrik du Toit [a], Maximilian O. Besenhard [a], Sultan Ben-Jaber [b], Peter Dobson [c], Ivan Parkin [b], Asterios Gavriilidis [a,*]

[a] Department of Chemical Engineering, University College London, Torrington Place, London WC1E 7JE, United Kingdom
[b] Department of Chemistry, University College London, 20 Gordon Street, London WC1H 0AJ, United Kingdom
[c] Warwick Manufacturing Group, University of Warwick, Coventry CV4 7AL, United Kingdom

HIGHLIGHTS

- Sub-3 nm gold nanoparticles were synthesized in continuous flow capillary reactors.
- Negatively charged capillary-solution interface offered enhanced nucleation rate.
- Gold nanoparticles with a weaker capping agent provided higher SERS signal.

ARTICLE INFO

Article history:
Received 25 January 2018
Received in revised form 16 June 2018
Accepted 19 June 2018
Available online 19 June 2018

Keywords:
Microreactors
Gold nanoparticles
Citrate reduction
Nucleation enhancement
Wall effects

ABSTRACT

Ultrasmall gold nanoparticles were synthesized without strong capping agents by using a capillary-based continuous flow system. A mixture of gold(III) chloride trihydrate and trisodium citrate flowed through capillaries at elevated temperature. The effect of capillary material (polytetrafluoroethylene, fluorinated ethylene propylene, polyetheretherketone, fused silica), surface-to-volume ratio (capillary internal diameter 0.3–1 mm), average residence time (1.5–30 min) and temperature (70–100 °C) were investigated. At a flow rate of 0.006 ml/min (residence time 30 min), 100 °C, 275 kPa back pressure, citrate/gold molar ratio 3.15 and using PTFE capillary tubing with an inner diameter of 0.3 mm, very small (1.9 ± 0.2 nm) nanoparticles were obtained. For comparison, experiments were also performed under the same experimental conditions, but in slug flow using octane as segmenting fluid, thus isolating the reactants from the tubing wall. The synthesized particles were 17.4 ± 1.4 nm for segmented flow, demonstrating the important effect of the capillary wall surface. The performance of these citrate-capped gold nanoparticles was tested for Surface-Enhanced Raman Scattering (SERS). The average enhancement factor (AEF) of 2 nm gold nanoparticles capped by citrate from our work (AEF = 1.54×10^8) was nearly double when compared to 2 nm phosphate-capped commercial gold nanoparticles (AEF = 7.34×10^7). The adsorption of analyte molecules onto citrate-capped gold surface was easier due to the weaker binding strength of the carboxylate ligand and more hotspots formed with narrower gaps between neighbouring particles, giving rise to improved enhancement.

This work has been selected by the Editors as a Featured Cover Article for this issue.

1. Introduction

With the intriguing physicochemical, nontoxic, biological and catalytic properties and the ease of functionalization, gold nanoparticles have attracted a lot of interest and have many potential applications, e.g. catalysis (Ansar et al., 2017; Haruta et al., 1989), medical diagnosis (Huang et al., 2007), biomedical imaging (Chen et al., 2013; Howes et al., 2014), therapeutics (Dykman and Khlebtsov, 2011), analytical sciences (Daniel and Astruc, 2003). The production of gold nanoparticles with a size of approximately 15 nm from the reduction of tetrachloroauric acid by trisodium citrate at high temperatures was proposed by Turkevich in 1951 (Turkevich et al., 1951). In this method citrate has three roles during synthesis: a reducing agent, a capping agent and a pH mediator (Ji et al., 2007). However, because of the complex equilibrium of reactant species and parallel side reactions, the predominant parameter to control particle size is still disputed, and most mechanistic studies have been conducted in poorly characterised batch systems. A study by Kumar et al. concluded that the dicarboxy

* Corresponding author.
E-mail address: a.gavriilidis@ucl.ac.uk (A. Gavriilidis).

https://doi.org/10.1016/j.ces.2018.06.050
0009-2509/

acetone (DCA) formed from citrate reduction plays a predominant role which aids nucleation and its side product, acetone, could continue reducing the gold nanoparticles precursor and speed up growth (Kumar et al., 2006). Even though the model agreed with several literature results, it does not yield satisfactory predictions in other cases, because it does not take account of the acid-base properties of the reactants (Agunloye et al., 2017). Wuithschick et al. (2015) demonstrated experimentally that the Au(III) species are the critical element to control particle size. In their study, the formation of monodispersed gold nanoparticles in the Turkevich method was investigated. When the initial pH of the gold precursor is in the range of 2.7–4, a shift of equilibrium to the gold species with less reactivity occurs when changing the pH by adding citrate. When $[AuCl_4]^-$ ions are totally converted into hydroxylated species, nucleation stops, and the rest of gold ions are consumed for growth. Based on this hypothesis, Wuithschick et al. reversed the addition order of the reactants to add gold precursor to boiled citrate instead of adding citrate to boiled gold precursor proposed in the Turkevich method. As the gold precursor has a higher concentration, which is associated with lower pH and the presence of more $[AuCl_4]^-$ at the early stages, the final particle size obtained by the inverse Turkevich method could be as low as 7.6 nm without any additional strong reducing agents or ligands.

It has been established that fast nucleation is the key in order to achieve monodispersed and small gold nanoparticles (Wuithschick et al., 2015). However, since citrate is a moderately weak reducing agent, the nucleation rate using citrate reduction is not as fast as with some strong reducing agents such as $NaBH_4$. That is why the typical minimum nanoparticle diameter is in the range of 7 nm (Wuithschick et al., 2015). However, the low toxicity (Murphy et al., 2008) and the ease with which such citrate-capped gold nanoparticles can be functionalised, keeps researchers motivated to improve this method. This is also the reason why the current study has focused on a citrate-only system. In order to decrease the overall size and particle size distribution of the citrate-capped gold nanoparticles, several approaches have been implemented, such as using a stronger reducing agent (Brown et al., 1996; Piella et al., 2016; Singh et al., 2009; Slot and Geuze, 1985), tuning citrate concentration (Kimling et al., 2006), reaction temperature (Wuithschick et al., 2015), solution pH (Ji et al., 2007), reactant pre-mixing at room temperature, adding Ag^+ ions (Xia et al., 2009), employing UV irradiation (du Toit et al., 2017) and ultrasound (Su et al., 2003). In batch systems, it seems that only with a stronger reducing agent can the size of citrate-capped gold nanoparticles be made smaller than 5 nm.

Microreactors have many advantages over batch reactors, such as better mixing, enhanced mass and heat transfer (Shahbazali et al., 2014), high surface-to-volume ratios, easier and safer control of different process parameters of the process and they are potentially easier to scale up (Zhang et al., 2017). Thus, many researchers have adopted the use of microreactors for the production of citrate-capped gold nanoparticles. In most cases researchers take advantage of better mixing in different types of microreactors (Kumar et al., 2014; Liu et al., 2015; Sugano et al., 2010; Yang et al., 2010) in order to reduce the polydispersity of synthesized gold nanoparticles and tune the particle size by parameter optimization (Lohse et al., 2013). Nonetheless, without strong reducing agents, faster mixing itself cannot fundamentally increase nucleation rate. Thus, the final size of the particles could only be reduced to around 7 nm (Wuithschick et al., 2015). It is noteworthy that (Ftouni et al., 2012) produced ultrasmall size gold nanoparticles of mean diameter 1.8 nm at a residence time of 47 s in a citrate-only system by taking advantage of the short mixing, heating and quenching times in a continuous flow capillary reactor. As the residence time was quite short and the product could be quenched to terminate the reaction, no further growth after the formation of seed particles leads to this result, which is also the smallest particle size obtained by a citrate-only reduction so far. However, it is likely that not all the gold precursor was used, since it has been shown that only 1–2% of the gold precursor is consumed in the process of seed particle formation (Wuithschick et al., 2015). If that was the case, most of the gold precursor would not have been utilised, while unconsumed $HAuCl_4$ in the product could lead to instability of particle size.

One of the most widely used methods to synthesize gold nanoparticles under 5 nm is the Brust-Schiffrin method which involves both a strong reducing agent ($NaBH_4$) and a capping agent with a strong binding strength (namely thiols) (Brust et al., 1994). As $NaBH_4$ keeps reducing unconsumed Au(III), nuclei are produced throughout the whole synthesis which leads to overlapping of nucleation and growth processes. In this case the thiol plays a decisive role to separate synthesized gold nanoparticle efficiently and thus limit the growth of particles. This is why most of gold nanoparticles with ultrasmall size are stabilized by thiols. However, thiols are not vital to stabilize ultrasmall gold nanoparticles. As a stabilizing agent, citrate has been shown to be capable of stabilizing gold nanoparticles of ca. 3.5 nm (Piella et al., 2016). Thus, in order to synthesize sub-5 nm gold nanoparticles reduced by citrate, the key point is the enhancement of the nucleation rate, as the final particle size can be determined by the amount of nuclei formed. Under high nucleation rates, more nuclei are produced and thus less gold precursor is available for growth.

In the present study we test the feasibility of a new approach to enhance nucleation rate by using the surface interaction between reactants and the negatively-charged tubing wall of different capillary microreactors. A low flow rate ensures enough time for surface interactions to consume the entire gold precursor. The size of the synthesized citrate-capped gold nanoparticles could thus be reduced below 3 nm. The particles obtained show a better SERS performance compared to phosphate-capped gold nanoparticles with similar size.

2. Experimental

The experimental set-up shown in Fig. 1 was based on circular capillary microreactors (length 2.5 m) with different internal diameter (I.D.) and of different materials: polytetrafluoroethylene (PTFE, 0.3–1.0 mm I.D.), fluorinated ethylene propylene (FEP, 0.25 mm I.D.), polyetheretherketone (PEEK, 0.25 mm I.D.) (from SUPELCO) and fused silica (0.32 mm I.D. from Polymicro Technologies). It also employed a micromixer chip (Dolomite, Part No. 3000144), a stirred glycerol (99.5%,VWR) bath on a hot plate (Stuart, UC152D with SCT temperature controller) to keep the microreactor temperature at 70–100 °C, a double syringe pump (Harvard PhD Ultra), a sample and waste collection unit (including two 4 ml cuvettes and a 700 ml steel vessel) with back pressure

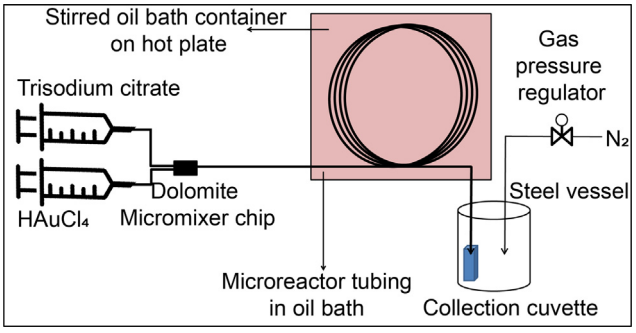

Fig. 1. Experimental set-up of continuous flow synthesis of ultrasmall gold nanoparticles in capillary tubing using chloroauric acid and trisodium citrate.

regulator (Swagelok, SPL Back Pressure Regulator, max pressure 1000 kPa) adjusted to 275 kPa to supress boiling.

In a typical synthesis procedure Gold(III) chloride trihydrate (Sigma-Aldrich, $\geq$ 99.9%) and trisodium citrate (Sigma-Aldrich, $\geq$ 99%) were dissolved in deionized water (15 MΩ·cm). All the reagents were filtered (GVS Filter Technology, Polyethylene, 0.2 μm) before pumping into tubing made of different materials and I.D.s. The $HAuCl_4$ and trisodium citrate solutions were injected through two glass syringes using the double syringe pump at a constant volumetric flow ratio of 1. Freshly prepared aqua regia and then deionized water water were used to clean the system after every experiment. For slug flow experiments a stream of pure octane (Sigma-Aldrich, $\geq$ 99.9%) and the aqueous reactant mixture (1/1 citrate/gold volumetric flowrate ratio) were merged in a T-mixer (IDEX Health & Science LLC, 0.5 mm through hole), at 1/1 organic/aqueous volumetric flowrate ratio. Slug flow was used to prevent the interaction between reagents and PTFE tubing wall by forming a thin lubricating layer between the droplets and tubing wall. All the parameters used for the slug-flow experiment were kept constant (0.3 mm I.D. PTFE tubing, average residence time of 30 min, temperature of 100 °C, 275 kPa back pressure and citrate/gold molar ratio of 3.15).

UV–Vis absorption spectra of gold nanoparticle solutions were recorded using an Ocean Optics UV–Vis-ES spectrometer (USB 2000 + Spectrometer and DT-Mini-2-GS light source). The spectra were recorded immediately after the experiments and the samples for transmission electron microscopy (TEM) analysis were prepared concurrently. TEM images and selected area electron diffraction (SAED) analysis were taken on a JEOL 2100 EXii microscope with a 120 kV acceleration voltage. TEM samples were prepared by dipping a drop of the colloidal solution onto lacey carbon film on a 400 mesh copper grid (E M Resist Ltd) and allowed to dry in air. The polydispersity of the synthesized particles is defined as the standard deviation of the particle size distribution. Scanning electron microscope (SEM) images of the inner surface of the capillary tubing were taken on a JEOL JSM-6701F microscope. X-ray photoelectron spectroscopy (XPS) was performed using a Thermo Scientific K-alpha photoelectron spectrometer using monochromatic Alkα radiation. Higher resolution scans were recorded for the principal peaks of Au(4f) and C(1s) at a pass energy of 50 eV. The peaks were modelled using CasaXPS software with binding energies adjusted to adventitious carbon (284.8 eV) for charge correction. ATR-FTIR spectroscopy was performed using a Perkin-Elmer 1605 FT-IR spectrometer with a resolution of 0.5 cm^{-1} and wavenumber range 500–4000 cm^{-1}. Inductively coupled plasma atomic emission spectroscopy (Varian 720 ICP-AES, axial configuration) was used to measure the gold amount of synthesized ultrasmall gold nanoparticles. 1 ml product solution was centrifuged at speed of 100,000 rpm for 1 h by ultracentrifuge (Beckman Coulter, Optima MAX) to precipitate the particles. Subsequently, both the precipitate and supernatant were digested by aqua regia and diluted to 5 ml. The yield was calculated by the amount of gold in the precipitate detected by ICP-AES over the original amount of gold precursor.

Raman signals were measured with a Renishaw Raman inVia microscope with a 633 nm He-Ne excitation laser (1.9 eV, 0.7 mW, pore size ~4.4 μm^2). A comparison of Surface-Enhanced Raman Scattering (SERS) performance between our synthesized citrate-capped gold nanoparticles from fused silica tubing and gold colloid stabilized in phosphate buffered saline (PBS) buffer solution with similar particle size (2 nm, EM.GC2, BBI Solutions) was carried out. 10^{-5} M of the aqueous analyte Rhodamine-6G was mixed with the same volume of gold nanoparticle solution and then stirred for 20 min to leave enough time for the molecules to bind onto the gold surface. The solutions were then drop-cast onto glass substrate to dry and create SERS hotspots.

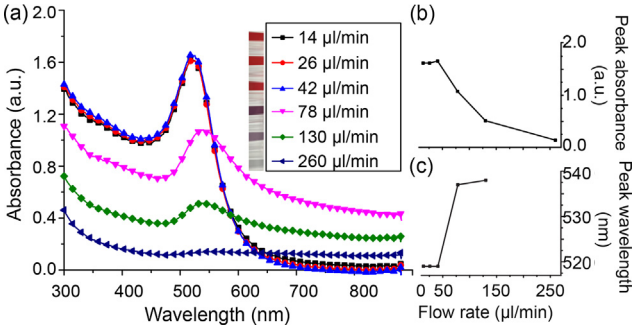

Fig. 2. (a): UV–vis spectra of gold nanoparticles synthesized in PTFE tubing with an I.D. of 0.5 mm, at temperature of 80 °C and total flow rates as indicated, corresponding to average residence times 1.5–30 min. Inset: colour of the products at different flow rates. (b): Maximum peak absorbance of gold nanoparticle solutions at various flow rates from UV–Vis spectroscopy. (c): Wavelength of maximum absorption (λ_{max}) at various flow rates. Solutions of 1.08 mM $HAuCl_4$ and 5.4 mM citrate were mixed at 1/1 volumetric flowrate ratio.

The zeta potential of the four different tubing materials was determined using the SurPASS 3 (Anton Paar) electro-kinetic analyser for macroscopic solids based on a streaming potential measurement. Tubing samples were measured using the SurPASS 3 measuring cell for flexible tubing. 1 mM KCL solutions were used for all measurements. Further details on the performed zeta potential analysis can be found in the Supporting Information.

3. Results and discussion

3.1. Influence of flow rate

The flow rate in our study was low as we aimed to provide more opportunity for surface interaction between the reagents and the tubing wall and consume all of the Au(III) within the microreactor leading to a more stable product. The dispersion number was <0.01 for the various components and capillaries used in the experiments (see details in Table S1, Supporting Information), which indicates practically plug flow behaviour (Levenspiel, 1999). Thus, it is expected that slow flow rate would not alter nanoparticle size distribution.

The initial concentration of $HAuCl_4$ after mixing was kept relatively high at 0.54 mM to facilitate UV–Vis measurements. The I.D. of the PTFE tube used for these experiments was 0.5 mm. Under these conditions, products with different colours were synthesized as shown in Fig. 2(a). By changing the inlet flow rate, the product exited the microreactor after a residence time of 1.5–30 min. The colour of the product obtained depended on the residence time. The microreactor product colour changes shown in Fig. 2(a) inset show the same trend as observed in a batch system as a function of synthesis time; from blue to purple to red[1] as reaction progresses (Turkevich et al., 1951). The different colours represent different stages of the nucleation and growth processes. The above indicate that the microreactor system did not change the general reaction pathway of the Turkevich method. With the first three flow rates used (14, 26, and 42 μl/min), the peak absorption of the obtained solutions nearly overlapped, which indicates that the flow rate did not have a big effect on gold nanoparticle synthesis, provided enough time was allowed in the reactor to complete particle growth. Fig. 2(b) shows that the peak absorbance, which is related to the final concentration of the product (Haiss et al., 2007), was influenced by flow rate. There was overall a decreasing trend of absorbance as flow rate increased. For flow rates >50 μl/min, the residence time was too short for the reduction, and unconsumed

[1] For interpretation of color in Fig. 2, the reader is referred to the web version of this article.

gold precursor in solution led to the low absorbance in UV–Vis. Fig. 2(c) indicates the effect of flow rate on wavelength of maximum absorption (λ_{max}), which is related to gold nanoparticle particle size (Haiss et al., 2007). As it is very hard to identify a peak for the sample at the highest flow rate (260 μl/min), there is no data presented for this condition. For flow rates <50 μl/min, the solutions had the same $\lambda_{max,}$ which indicates nanoparticles that did not change in size. No further growth was observed with increasing residence time between the flow rate of 42 μl/min and 14 μl/min. For this reason, all subsequent experiments were performed with low flow rates. The increasing λ_{max} at higher flow rates (78–260 μl/min), which is associated with colour change from purple to red, has been investigated by several groups (Chow and Zukoski, 1994; Ji et al., 2007; Pei et al., 2004; Pong et al., 2007; Rodríguez-González et al., 2007) and attributed to aggregate formation at the early stages of the synthesis. However, recent research suggests that it could probably be caused by the attachment of gold ions on the surface of nuclei (Polte, 2015).

3.2. Synthesis of ultrasmall size gold nanoparticles

The bottleneck of synthesizing sub-5 nm gold nanoparticles in the Turkevich method is the slow nucleation rate obtained by the moderately weak reducing strength of the citrate. If the nucleation rate could be enhanced, gold nanoparticles of smaller size would be expected. Turkevich et al. (1951, 1953) suggested that in citrate reduction, the dicarboxyacetone (DCA) formed from trisodium citrate by thermal decomposition or reduction reaction acts as an organizer to assemble gold ions in a form of multi-molecular complex. The increasing local concentration of precursor facilitates the reduction of Au(III) (Turkevich et al., 1953). The nucleation rate is reportedly enhanced if another stronger organizer (which plays a similar role to DCA) is used.

It has been demonstrated that in the layer-by-layer process (a thin film fabrication technique), oppositely charged reactants and polymers form multiple layers of inorganic–polymer by electrostatic attraction (Caruso et al., 1998). By making use of this feature Ma et al. (2015) improved the catalytic performance of gold nanoparticles with the aid of polydopamine (PDA) nanoparticles (~200 nm) compared with the same amount of gold nanoparticle suspension. In their study, PDA carriers with negative charge increased the concentration of positively charged reactant for the loaded catalysts (gold nanoparticles) on the carriers due to the electrostatic attraction.

Inspired by this concept, we used the tubing wall of the microreactor as an organizer to increase the local concentration of Au(III) and thus enhance the nucleation rate. Because of the large surface-to-volume ratio, the interaction between reactants and tubing wall was enhanced compared to a batch reactor system. Fig. 3 proposes a possible process which enhances the nucleation rate in this study. The $HAuCl_4$ and trisodium citrate are premixed at room temperature before being pumped into the microreactor system. Initially positively charged citrate-gold ion complexes are formed (Yang et al., 2007). The tubing wall with negative surface potential increases the local concentration of opposite charged citrate-gold ion complexes by electrostatic attraction (Ma et al., 2015). As the increasing concentration of gold precursor accelerates the nucleation rate (Polte et al., 2010), more seed gold nanoparticles are formed which is expected to lead to smaller final nanoparticle size (Wuithschick et al., 2015). Once gold nanoparticles are synthesized and capped with citrate, they become negatively charged (Park and Shumaker-Parry, 2014). With the resulting electrostatic repulsion gold nanoparticles could be repelled from the wall and transfer back into the bulk solution without further attachment on the tubing wall. As it will be shown later, this is only partly successful and a portion of nanoparticles irreversibly attach on the wall giving rise to fouling. After the entire gold precursor is consumed, no electrostatic attraction exists. This is consistent with the fact that no fouling was observed on the latter section of tubing, because of repulsion between stabilized gold nanoparticles and tubing wall with the same charge.

In order to adsorb positively charged citrate-gold complexes, the tubing wall must carry negative charge; the latter depends on the pH of solution (Kirby and Hasselbrink, 2004). However, the Turkevich method is a pH-dependent reaction (Ji et al., 2007). In the experiments in this section, the initial concentration of precursor before mixing was 0.54 mM (with initial pH of 3.3), which is in the optimal pH range of 2.7–4 proposed for the synthesis of monodispersed gold nanoparticles by citrate reduction (Wuithschick et al., 2015). At a citrate to gold precursor ratio of 3.15, the final pH of the solution is around 6. PTFE has a negative surface potential at this pH (Kolská et al., 2013). The inner tubing diameter was small, at 0.3 mm, in order to provide more opportunity for surface interaction between the solution and tubing wall. In order to consume all the gold precursor, synthesis was conducted using low total flow rate (6 μl/min).

A colourless product which did not exhibit a Localized Surface Plasmon Resonance (LSPR) band was obtained, indicating gold nanoparticles with diameter below 3 nm (Buining et al., 1997). The TEM image shown in Fig. 4(a) verified that the colourless solution contained gold nanoparticles with ultrasmall size of 1.9 ± 0.2 nm (12.8%). The high magnification HR-TEM image in Fig. 4(b) shows a gold nanoparticle with lattice spacing consistent with Au (Lind, 1983). The selected area electron diffraction (SAED) pattern in Fig. 4(c) is diffuse due to the small diameter of gold nanoparticles (Ftouni et al., 2012).

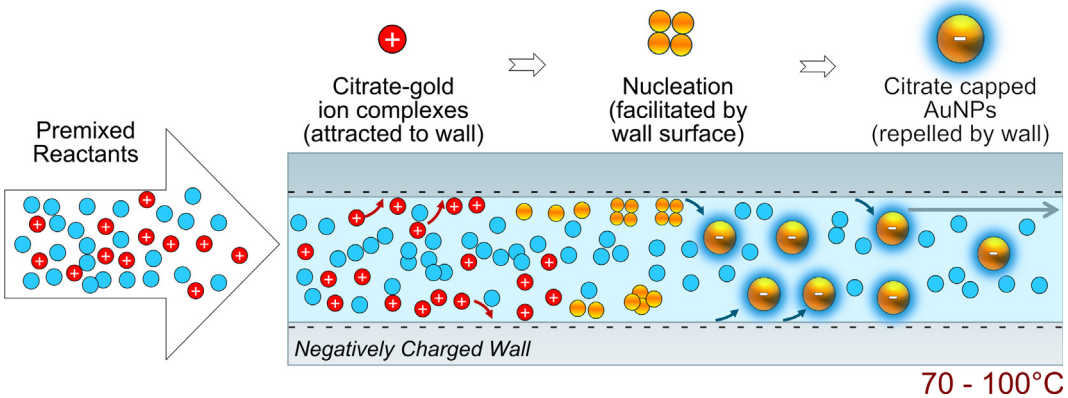

Fig. 3. Schematic illustration of the enhancement of nucleation during gold nanoparticle synthesis by surface interaction between the reactants and the microreactor wall.

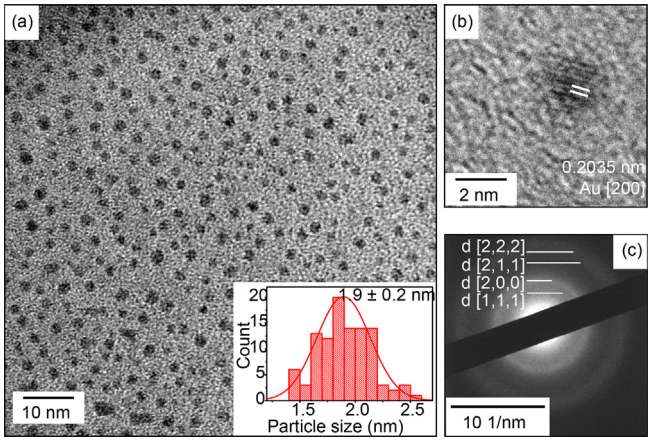

Fig. 4. TEM images of gold nanoparticles synthesized with total flow rate of 0.006 ml/min (residence time 30 min), at 100 °C using PTFE capillary tubing with an I.D. of 0.3 mm. (a) Colourless product of gold nanoparticles with a size of 1.9 ± 0.2 nm (polydispersity 12.7%) (b) High magnification HR-TEM image showing a gold nanoparticle with the inter-planar spacing in the [2 0 0] direction. (c) SAED pattern of the gold nanoparticles synthesized. Solutions of 0.54 mM $HAuCl_4$ and 1.7 mM citrate were mixed at 1/1 volumetric flowrate ratio.

With time, a section of "dark fouling" followed by "pink fouling" was observed near the inlet of the PTFE tube (Fig. S1). This seems to be congruent with the blue colour appearing during citrate reduction. Moreover, this so-called "dark fouling" was not firmly attached like the "pink fouling" (the "dark fouling" was quite easily removed by increasing the flow rate, while the "pink fouling" could only be removed by aqua regia). Polte and co-workers showed that the blue colour during the early stages of gold nanoparticle synthesis by citrate reduction was not due to particle aggregation, as no significant scattering signal was detected by ultrasmall angle X-ray scattering (USAXS) (Wuithschick et al., 2015). In their study, they proposed that this blue colour was due to the attachment of gold ions in an electric double layer, resulting in a change of plasmonic properties (Polte, 2015). The characterization of the "dark fouling" by XPS and IR (Fig. S2 in Supplementary Information) showed the co-existence of Au(0) and unconsumed gold ions, as well as a high amount of citrate-gold complex. As this material was observed at the tubing surface, the "dark fouling" is supportive evidence for nucleation sites and adsorption of gold ions around the tubing wall, caused possibly by electrostatic attraction. With decreasing concentration of gold ions along the reactor, the colour of the fouling changed to pink indicating gold nanoparticles irreversibly attached on the tubing wall, most probably by van der Waals forces.

3.3. Influence of tube surface-to-volume ratio

To demonstrate that the PTFE tubing wall plays a crucial role in obtaining ultrasmall particles, experiments with the same length (2.5 m) but different inner tube diameters and hence surface-to-volume ratios were carried out. Fig. 5 shows TEM images of the synthesized gold nanoparticles (Fig. 5a–d) and the trend of nanoparticle size obtained as a function of the reactor surface-to-volume ratio (Fig. 5e). The diameter of the synthesized gold nanoparticle obtained from slug flow when the surface-to-volume ratio is zero was 17.4 ± 1.4 nm (8.2%). This is in the typical size range for gold nanoparticles synthesized in batch by the Turkevich method (e.g. 17.4 nm with polydispersity of 10% in Wuithschick et al., 2015). The result indicates that without interaction between reagents and the tubing wall, there was no enhancement of nucleation, even though a small tube (0.3 mm I.D.) was used. The segmented flow microfluidic system has

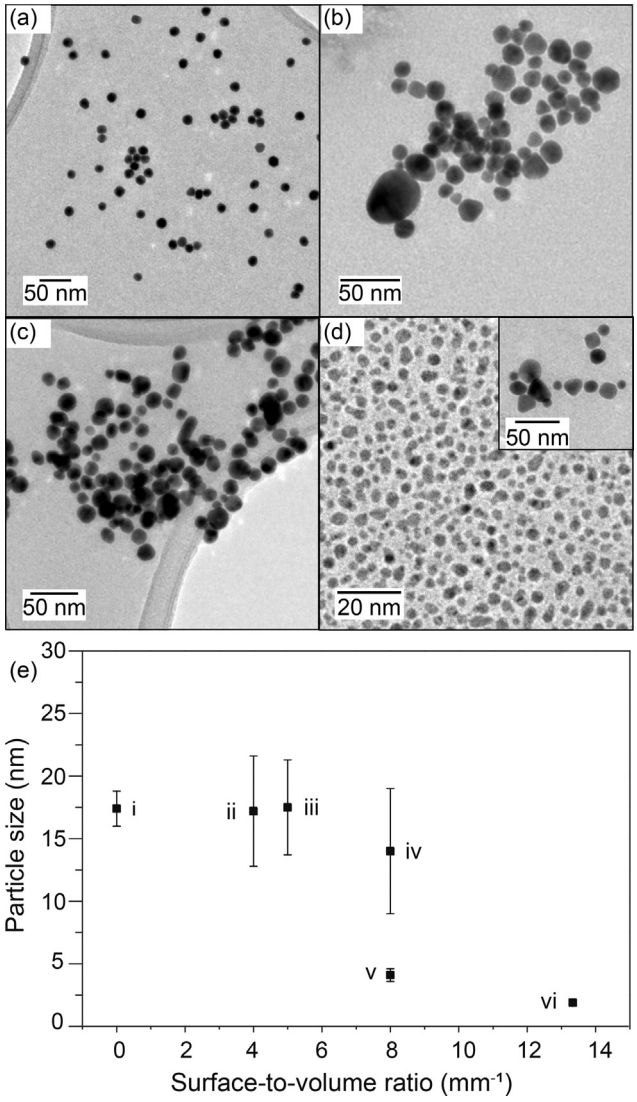

Fig. 5. TEM images of gold nanoparticles synthesized at the same average residence time (30 min), with PTFE tubing of varying I.D. at 100 °C. (a) Aqueous phase segmented by octane in capillary with an I.D. of 0.3 mm, and single-phase flow in capillary with I.D. of (b) 1 mm, (c) 0.8 mm, (d) 0.5 mm. The insert shows the larger size gold nanoparticles found on another area of the same TEM grid of (d). (e) Nanoparticle size obtained as a function of the reactor surface-to-volume ratio from (i) slug flow, (ii) 1 mm I.D. tube, (iii) 0.8 mm I.D. tube, (iv) and (v) 0.5 mm I.D. tube and (vi) 0.3 mm I.D. tube in Fig. 4. Error bars represent the standard deviation of nanoparticle size distribution. Solutions of 0.54 mM $HAuCl_4$ and 1.7 mM citrate were mixed at 1/1 volumetric flowrate ratio.

sufficient mixing and narrow residence time distribution to achieve low polydispersity of particle size. When the solution of reactants was in contact with the tubing wall, the wall nucleation rate was enhanced. With increasing the I.D. (0.5 mm, 0.8 mm and 1 mm) the surface-to-volume ratio decreased, and the bulk nucleation was dominant at large tube sizes rather than enhanced nucleation by the tubing wall. For the gold nanoparticles synthesized with the 1 mm tube (Fig. 5b), a mean particle size of 17.3 ± 4.5 nm (polydispersity 25.8%) was obtained and for the 0.8 mm tube (Fig. 5c), it was 17.5 ± 3.8 nm (polydispersity 21.7%). In both cases the particle size distribution was broader compared to slug flow synthesis (Fig. 5a, 17.4 ± 1.4 nm, 8.2%); this is in accordance with the broader particle size distribution that He et al. (2005) observed when bulk solution interacted with the tubing wall. We propose that this broad size distribution is due to the fact that even though surface interaction still existed in these two cases, the

amount of gold ions adsorbed by the tubing wall was proportionally small. The rest of the gold ions were reduced in the bulk fluid. Two nucleation processes with different rates occurred at the same time which affected the separation of nucleation and growth. For the 0.8 and 1 mm capillaries, the gold nanoparticles obtained were more polydisperse than the classical citrate reduction. In contrast, the wall surface of the 0.5 mm capillary started to affect nucleation and there were two different types of gold nanoparticles formed: polydisperse gold nanoparticles from uncontrollable growth and small gold nanoparticles with sizes of around 4.1 ± 0.5 nm (11.3%) (Fig. 5d). In this case, more citrate-gold complexes had the opportunity to interact with the tube surface and thus less precursor was left for bulk nucleation/growth. Hence, even though two nucleation processes took place, more Au(III) was consumed by enhanced nucleation at the wall because of the larger surface-to-volume ratio. Compared with gold nanoparticles synthesized in the 0.3 mm I.D. tubing, the particle size of small gold nanoparticles synthesized with the 0.5 mm I.D. tubing in Fig. 5d (insert) was larger, possibly because the amount of unconsumed gold precursor in the 0.5 mm tubing was higher than the 0.3 mm tubing. After the enhanced nucleation stage, the seed particles were repelled by the tubing wall and entered the flow for further growth. The larger amount of unconsumed gold precursor left in solution led to the larger particle size obtained after full growth. The large size particles disappeared when the surface-to-volume ratio was >13 (tubing with 0.3 mm I.D.) and monodisperse gold nanoparticles with ultrasmall size of 1.9 ± 0.2 nm were obtained (Fig. 4). It is worth noting that He et al. (He et al., 2005) obtained monodisperse silver nanoparticles using PTFE tubing with a very small I.D., and they also proposed the presence of enhanced nucleation at the tube surface.

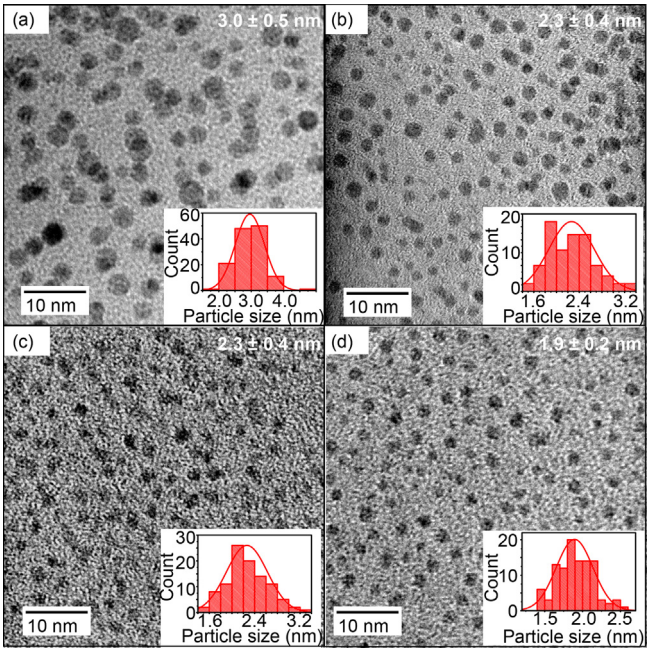

Fig. 6. TEM images of the gold nanoparticles synthesized at different temperature. (a) 70 °C, with size of 3.0 ± 0.5 nm, (b) 80 °C, with size of 2.3 ± 0.4 nm, (c) 90 °C, with size of 2.3 ± 0.4 nm, (d) 100 °C, with size of 1.9 ± 0.2 nm. PTFE tubing with 0.3 mm I.D. was used with total flow rate of 0.006 ml/min (average residence time 30 min). Solutions of 0.54 mM $HAuCl_4$ and 1.7 mM citrate were mixed at 1/1 volumetric flowrate ratio.

3.4. Influence of temperature

The effect temperature has on the gold nanoparticle size is dependent on a combination of different processes in the citrate reduction method. Firstly, the rate of gold ion reduction and formation of seed particles increases with increasing temperature, which leads to the formation of more nuclei. Secondly, increasing temperature promotes a shift of the gold precursor equilibrium to more hydroxylated species of $HAuCl_4$ which have lower reactivity, and thus lead to the formation of fewer nuclei (Wuithschick et al., 2015). These two opposite effects result in a non-monotonic trend of final particle size versus temperature depending on specific conditions. In the present study, gold nanoparticles were synthesized at temperatures of 70–100 °C in order to investigate the effect of temperature on this new synthesis approach. As shown in Fig. 6, the size and size distribution decreases with increasing temperature. The largest particle size obtained was 3.0 ± 0.5 nm at 70 °C, which is still small compared with the typical particle size in the Turkevich method. This suggests that the enhanced nucleation rate by the tubing wall plays a predominant role on particle size and the effect of the decreasing reactivity of hydroxylated gold precursor species is not affecting this synthesis. Furthermore, a higher temperature speeds up the reduction rate which also enhances the nucleation rate. Thus, the larger amount of gold atoms available during the nucleation stage produces more seed particles and the total precursor is distributed to more particles, resulting in smaller gold nanoparticles at higher temperature.

3.5. Influence of tube material

Based on the hypothesis above, the synthesized negatively-charged particles should be repelled from the wall; however, fouling issues were still present. We hypothesise that fouling is influenced by tubing roughness. Since rough surfaces have increased surface area on which particle nucleation can occur, there might be an excessively high level of nucleation occurring simultaneously. Liu et al. suggested that coarser polymeric tubes could provide more sites for nucleation due to larger superficial area. They observed that silver nanoparticles were more prone to depositing on the surface of a coarser tube and the nanoparticles also had larger average size and wider size distribution (Liu et al., 2012). The high concentration of nuclei can lead to the formation of larger particles by nuclei aggregation, which can foul prior to citrate stabilisation. The rough tube surface may also locally disrupt the near-wall flow potentially trapping particles, and increasing the probability of fouling on the wall. With longer operation time, fresh gold precursor passes over these particles causing them to grow and form fouling. Changing the tubing material could also change the zeta potential and surface charge of the tubing wall, resulting in different nucleation rates. Three other tubing materials, FEP (0.25 mm I.D.), PEEK (0.25 mm I.D.), and fused silica (0.32 mm I.D.), were tested at the same experimental conditions as PTFE (residence time of 30 min, 100 °C at citrate/gold molar ratio of 3.15). The relative roughness of these four materials as determined by SEM in Fig. S3) was found qualitatively to be PTFE > PEEK > FEP > fused silica, which is in accordance with the literature (Hecht, 2014).

Table 1 lists the zeta potential values at pH ~6.5 of the tested materials at room temperature, which are in good agreement with literature values. The pH dependent zeta potentials are shown in Fig. S5. All tested materials exhibited a negative zeta potential at process relevant pH values, and the most negative zeta potential was obtained for fused silica. Hydrophobic surfaces without functional groups, such as polymers, have negative surface potentials (at pH > 4, i.e. the typical isoelectric point for these surfaces) due to increased concentration of hydroxide ions rendering the surface charge negative. The zeta potential of the fused silica tubing is comparatively lower, because of ionisation of surface silanol

Table 1
Zeta potential values of tubing materials and comparison with literature values. Further details on the pH dependence are shown in Fig. S5.

Material	Zeta potential at pH ~6.5 from streaming potential	Zeta potential at pH ~6.5 literature
PTFE	−25 mV	−24 mV[a]
PEEK	−20 mV	−22.5 mV[b]
FEP	−28 mV	–
Fused silica	−88 mV	−100 mV[c]

[a] Werner et al. (1999).
[b] Bismarck et al. (1999).
[c] Schwer and Kenndler (1991).

groups. Thus, the different characteristics of the tubing material result to different electrostatic attraction and therefore different nucleation rates. It is noteworthy that the zeta potential is expected to be more negative at higher temperatures (Evenhuis et al., 2006).

Fig. 7 shows the average gold nanoparticle size obtained at different operation times with different tube materials (size obtained from TEM images (Fig. S6)). As all the capillaries were negatively charged and nucleation rates were enhanced, they all produced ultrasmall gold nanoparticles of ~2–3 nm. The particle sizes did not change much with increasing operation time, which is in accordance with the conclusion obtained from Fig. 2, i.e. that the fouling did not affect the particle size to a great extent, as was also observed by Wagner and Köhler (2005). However, for the FEP tubing, there were some larger size particles (FEP_2 in Fig. 7) together with small size particles (FEP_1 in Fig. 7). Compared to the PTFE tubing, the FEP tubing has a smoother surface, so it is postulated that when the particles on the tube wall grow to a large size, it is harder to be held on the surface of FEP tubing than PTFE tubing; hence some large particles come out with the flow. The yield of the gold nanoparticles (Fig. S7) obtained with all tubing materials decreased with longer operation time, as more Au(III) was consumed and fouling on the wall increased (the loss originated from fouling, as there was no gold detected by ICP in the supernatant after centrifugation). The highest yield of 29.1% obtained (FEP tubing with operation time of 6.5 h) could be attributed to the presence of large particles (FEP_2 in Fig. 7). This is the reason why yield sharply decreased as the size of large particles at different operation time decreased. The fused silica produced the smallest particle size with high yield (23.1%) although the inner tube diameter was not the smallest, possibly because its zeta potential was the most negative. Even though the surface of fused silica was also very smooth, the highly negative zeta potential guaranteed a fast nucleation and that less precursor was left for growth or fouling. During the first 23 h of operation time, there was no sharp decrease of the yield, indicating that the rate of fouling was slower than other tubing materials.

3.6. SERS experiments with ultrasmall gold nanoparticles

Surface-enhanced Raman Scattering (SERS) is widely used in analytical chemistry for the detection of molecules with strong enhancement of Raman signals by absorbing the molecules onto metal surfaces (e.g. gold nanoparticles) (Ben-Jaber et al., 2016; Le Ru and Etchegoin, 2008; Le Ru and Etchegoin, 2012; Li et al., 2010). The enhancement of the signals is mainly caused by two effects: electromagnetic (EM) enhancement and a chemical contribution (Osawa and Ikeda, 1991). Compared with EM enhancement, the charge transfer-based chemical contribution provides a much smaller enhancement and the actual mechanism is still in dispute (Otto, 2005; Otto et al., 1980; Tognalli et al., 2011). The electromagnetic enhancement utilizes the LSPR of nanostructures to form incident electric field which could drive the conduction electrons. Thus, the EM enhancement is strongly affected by the morphology of the noble-metal structures (Juvé et al., 2013). Additionally, the EM enhancement decays exponentially with the distance between the metal surface and analyte molecules (Le Ru and Etchegoin, 2008). As mentioned above, the citrate on electrostatically stabilized citrate-capped gold nanoparticles can be easily removed for further functionalization, resulting in closer and easier interaction between the metal surface and analyte molecules. Even though the gold nanoparticles used for SERS are usually in the size range of 20–100 nm (Jana and Pal, 2007), the aggregation caused by mixing the analyte with 2 nm gold nanoparticles could increase the hot-spot population on the substrate that give rise to SERS enhancement. A comparison of SERS performance between our synthesized citrate-capped gold nanoparticles from fused silica tubing (corresponding to Fig. 7) and commercial phosphate-capped gold nanoparticles with similar particle size (~2 nm) was carried out. The original Raman spectra of 5×10^{-6} M Rh6G solution without gold nanoparticles is shown as the red curve in Fig. 8. For the concentration of 5×10^{-6} M, the "signature" bands

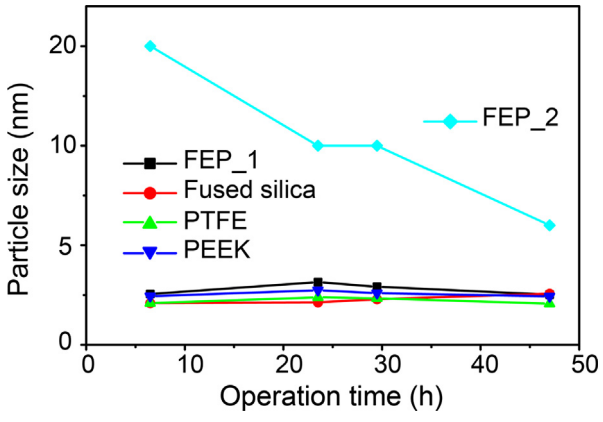

Fig. 7. Size of gold nanoparticles synthesized at average residence time of 30 min and 100 °C using different tube materials (FEP (0.25 mm I.D.), PTFE (0.3 mm I.D), PEEK (0.25 mm I.D.) and fused silica (0.32 mm I.D.)). Samples were collected at different operation times. FEP_1 and FEP_2 correspond to different types of particles observed on the same TEM grid obtained from FEP tubing. Solutions of 0.54 mM $HAuCl_4$ and 1.7 mM citrate were mixed at 1/1 volumetric flowrate ratio.

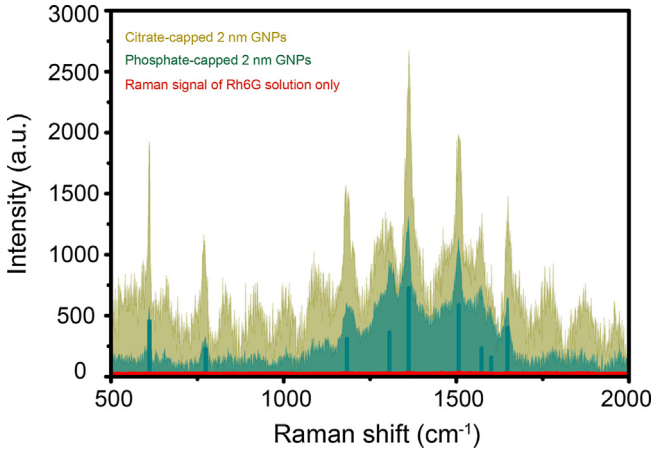

Fig. 8. Raman signal of Rh6G solution (red colour) and SERS spectra of Rh6G-tagged gold nanoparticles from citrate-capped gold colloid (sage colour) and phosphate-capped gold colloid (green colour) with similar size of 2 nm. (For interpretation of the references to colour in this figure legend, the reader is referred to the web version of this article.)

of Rh6G are hard to see. Fig. 8 indicates that both 2 nm gold nanoparticle samples could enhance Raman bands of Rh6G, as most of the molecule bands were successfully observed. The average enhancement factors (AEF) based on three intensities under different vibrational shifts (611 cm^{-1}, 1359 cm^{-1} and 1509 cm^{-1}) for both gold nanoparticle samples are shown in Table S2. The AEF of 2 nm gold nanoparticles capped by citrate from our work (AEF = 1.54×10^8) is nearly double when compared to the phosphate-capped commercial gold nanoparticles (AEF = 7.34×10^7). This is attributed to the fact that the adsorption of analyte molecules onto citrate-capped gold surface is easier due to the weaker binding strength of the carboxylate ligand. Additionally, during the drying process, gold nanoparticles capped with the weaker capping agent could form hotspots with narrower gaps between neighbouring particles, which gives rise to improved enhancement (Zhang et al., 2011).

4. Conclusions

Sub-3 nm citrate-capped gold nanoparticles were synthesized in continuous flow capillary reactors by enhancing nucleation through interaction between reactants and the tubing wall. It is speculated that the negatively charged tubing-water interface, offers heterogeneous nucleation sites for positive charged citrate-gold precursor species, stabilizing the nuclei and inhibiting their growth. The change of the surface charge (from positive to negative) as gold ions form gold nanoparticles provides electrostatic repulsion to remove the synthesized gold nanoparticles from the tubing wall. Under our continuous flow experimental conditions, the effect of temperature becomes less important in defining the final particle size, as compared to the classical batch Turkevich method. One of the disadvantages of our method is that fouling was observed and could not be avoided. Among four different tubing materials we tried, fused silica tubing showed the highest productivity because of its low zeta potential and smooth inner surface, which decreased fouling. The SERS performance of these citrate-capped gold nanoparticles was evaluated. A higher enhancement factor was observed compared to commercial phosphate-capped gold nanoparticles, because of more "hot spots" forming from weaker capping agent (citrate)-capped gold nanoparticles. This study provides a new point of view about using the feature of high surface-to-volume ratio in microfluidic systems in the synthesis of gold nanoparticles.

Acknowledgements

This work was supported by EPSRC, UK (grant EP/M015157/1). HH acknowledges support from the program of China Scholarships Council. We would like to thank Thomas Luxbacher and Renate Kohl (Anton Paar, Austria) for their support with the zeta potential measurements of the tubing, and Dr Sanjayan Sathasivam and Jijia Xie (University College London) for their support with the XPS and IR measurements.

Appendix A. Supplementary material

Supplementary data associated with this article can be found, in the online version, at https://doi.org/10.1016/j.ces.2018.06.050.

References

Agunloye, E., Gavriilidis, A., Mazzei, L., 2017. A mathematical investigation of the Turkevich organizer theory in the citrate method for the synthesis of gold nanoparticles. Chem. Eng. Sci. 173, 275–286.
Ansar, S.M., Fellows, B., Mispireta, P., Mefford, O.T., Kitchens, C.L., 2017. pH triggered recovery and reuse of thiolated poly(acrylic acid) functionalized gold nanoparticles with applications in colloidal catalysis. Langmuir 33, 7642–7648.
Ben-Jaber, S., Peveler, W.J., Quesada-Cabrera, R., Cortés, E., Sotelo-Vazquez, C., Abdul-Karim, N., Maier, S.A., Parkin, I.P., 2016. Photo-induced enhanced Raman spectroscopy for universal ultra-trace detection of explosives, pollutants and biomolecules. Nat. Comm. 7, 12189.
Bismarck, A., Kumru, M.E., Springer, J., 1999. Characterization of several polymer surfaces by streaming potential and wetting measurements: some reflections on acid–base interactions. J. Colloid Interf. sci. 217, 377–387.
Brown, K.R., Fox, A.P., Natan, M.J., 1996. Morphology-dependent electrochemistry of cytochrome c at Au colloid-modified SnO_2 electrodes. J. Am. Chem. Soc. 118, 1154–1157.
Brust, M., Walker, M., Bethell, D., Schiffrin, D.J., Whyman, R., 1994. Synthesis of thiol-derivatised gold nanoparticles in a two-phase liquid–liquid system. J. Chem. Soc., Chem. Commun., 801–802
Buining, P.A., Humbel, B.M., Philipse, A.P., Verkleij, A.J., 1997. Preparation of functional silane-stabilized gold colloids in the (sub) nanometer size range. Langmuir 13, 3921–3926.
Caruso, F., Lichtenfeld, H., Giersig, M., Möhwald, H., 1998. Electrostatic self-assembly of silica nanoparticle-polyelectrolyte multilayers on polystyrene latex particles. J. Am. Chem. Soc. 120, 8523–8524.
Chen, H., Shao, L., Li, Q., Wang, J., 2013. Gold nanorods and their plasmonic properties. Chem. Soc. Rev. 42, 2679–2724.
Chow, M., Zukoski, C., 1994. Gold sol formation mechanisms: role of colloidal stability. J. Colloid Interf. Sci. 165, 97–109.
Daniel, M.-C., Astruc, D., 2003. Gold nanoparticles: assembly, supramolecular chemistry, quantum-size-related properties, and applications toward biology, catalysis, and nanotechnology. Chem. Rev. 104, 293–346.
du Toit, H., Macdonald, T., Huang, H., Parkin, I., Gavriilidis, A., 2017. Continuous flow synthesis of citrate capped gold nanoparticles using UV induced nucleation. RSC Adv. 7, 9632–9638.
Dykman, L.A., Khlebtsov, N.G., 2011. Gold nanoparticles in biology and medicine: recent advances and prospects. Acta Nat. 3, 34–55.
Evenhuis, C.J., Guijt, R.M., Macka, M., Marriott, P.J., Haddad, P.R., 2006. Variation of zeta-potential with temperature in fused-silica capillaries used for capillary electrophoresis. Electrophoresis 27, 672–676.
Ftouni, J., Penhoat, M., Addad, A., Payen, E., Rolando, C., Girardon, J., 2012. Highly controlled synthesis of nanometric gold particles by citrate reduction using the short mixing, heating and quenching times achievable in a microfluidic device. Nanoscale 4, 4450–4454.
Haiss, W., Thanh, N.T., Aveyard, J., Fernig, D.G., 2007. Determination of size and concentration of gold nanoparticles from UV-vis spectra. Anal. Chem. 79, 4215–4221.
Haruta, M., Yamada, N., Kobayashi, T., Iijima, S., 1989. Gold catalysts prepared by coprecipitation for low-temperature oxidation of hydrogen and of carbon monoxide. J. Catal. 115, 301–309.
He, S., Kohira, T., Uehara, M., Kitamura, T., Nakamura, H., Miyazaki, M., Maeda, H., 2005. Effects of interior wall on continuous fabrication of silver nanoparticles in microcapillary reactor. Chem. Lett. 34, 748–749.
Hecht, K., 2014. Microreactors for Gas/liquid Reactions: The Role of Surface Properties. Western Engineering Inc, KIT-Bibliothek.
Howes, P.D., Rana, S., Stevens, M.M., 2014. Plasmonic nanomaterials for biodiagnostics. Chem. Soc. Rev. 43, 3835–3853.
Huang, X., Jain, P.K., El-Sayed, I.H., El-Sayed, M.A., 2007. Gold nanoparticles: interesting optical properties and recent applications in cancer diagnostics and therapy. Nanomedicine 2, 681–693.
Jana, N.R., Pal, T., 2007. Anisotropic metal nanoparticles for use as surface-enhanced Raman substrates. Adv. Mater. 19, 1761–1765.
Ji, X., Song, X., Li, J., Bai, Y., Yang, W., Peng, X., 2007. Size control of gold nanocrystals in citrate reduction: the third role of citrate. J. Am. Chem. Soc. 129, 13939–13948.
Juvé, V., Cardinal, M.F., Lombardi, A., Crut, A., Maioli, P., Pérez-Juste, J., Liz-Marzán, L. M., Del Fatti, N., Vallée, F., 2013. Size-dependent surface plasmon resonance broadening in nonspherical nanoparticles: single gold nanorods. Nano Lett. 13, 2234–2240.
Kimling, J., Maier, M., Okenve, B., Kotaidis, V., Ballot, H., Plech, A., 2006. Turkevich method for gold nanoparticle synthesis revisited. J. Phys. Chem. B 110, 15700–15707.
Kirby, B.J., Hasselbrink, E.F., 2004. Zeta potential of microfluidic substrates: 1. Theory, experimental techniques, and effects on separations. Electrophoresis 25, 187–202.
Kolská, Z., Makajová, Z., Kolářová, K., Slepičková, N.K., Trostová, S., Řezníčková, A., Siegel, J., Švorčík, V., 2013. Electrokinetic potential and other surface properties of polymer foils and their modifications. Polymer Science. InTech.
Kumar, D.V.R., Kulkarni, A.A., Prasad, B.L.V., 2014. Microfluidic platform for continuous flow synthesis of triangular gold nanoplates. Colloids Surf. A 443, 149–155.
Kumar, S., Gandhi, K.S., Kumar, R., 2006. Modeling of formation of gold nanoparticles by citrate method. Ind. Eng. Chem. Res. 46, 3128–3136.
Le Ru, E., Etchegoin, P., 2008. Principles of Surface-Enhanced Raman Spectroscopy: and Related Plasmonic Effects. Elsevier.
Le Ru, E.C., Etchegoin, P.G., 2012. Single-molecule surface-enhanced Raman spectroscopy. Annu. Rev. Phys. Chem. 63, 65–87.
Levenspiel, O., 1999. The Convection Model for Laminar Flow, Chemical Reaction Engineering. John Wiley and Sons Ltd, United States of America, pp. 339–349.
Li, J.F., Huang, Y.F., Ding, Y., Yang, Z.L., Li, S.B., Zhou, X.S., Fan, F.R., Zhang, W., Zhou, Z. Y., Ren, B., 2010. Shell-isolated nanoparticle-enhanced Raman spectroscopy. Nature 464, 392–395.

Lind, C.J., 1983. Characterization of Mineral Precipitates by Electron Microscope Photographs and Electron Diffraction Patterns. United States Geological Survey, United States.
Liu, G., Yang, X., Li, Y., Yang, Z., Hong, W., Liu, J., 2015. Continuous flow controlled synthesis of gold nanoparticles using pulsed mixing microfluidic system. Adv. Mater. Sci. Eng.
Liu, H., Huang, J., Sun, D., Lin, L., Lin, W., Li, J., Jiang, X., Wu, W., Li, Q., 2012. Microfluidic biosynthesis of silver nanoparticles: effect of process parameters on size distribution. Chem. Eng. J. 209, 568–576.
Lohse, S.E., Eller, J.R., Sivapalan, S.T., Plews, M.R., Murphy, C.J., 2013. A simple millifluidic benchtop reactor system for the high-throughput synthesis and functionalization of gold nanoparticles with different sizes and shapes. ACS Nano 7, 4135–4150.
Ma, A., Xie, Y., Xu, J., Zeng, H., Xu, H., 2015. The significant impact of polydopamine on the catalytic performance of the carried Au nanoparticles. Chem. Commun. 51, 1469–1471.
Murphy, C.J., Gole, A.M., Stone, J.W., Sisco, P.N., Alkilany, A.M., Goldsmith, E.C., Baxter, S.C., 2008. Gold nanoparticles in biology: beyond toxicity to cellular imaging. Acc. Chem. Res. 41, 1721–1730.
Osawa, M., Ikeda, M., 1991. Surface-enhanced infrared absorption of p-nitrobenzoic acid deposited on silver island films: contributions of electromagnetic and chemical mechanisms. J. Phys. Chem. 95, 9914–9919.
Otto, A., 2005. The 'chemical' (electronic) contribution to surface-enhanced Raman scattering. J. Raman Spectrosc. 36, 497–509.
Otto, A., Timper, J., Billmann, J., Kovacs, G., Pockrand, I., 1980. Surface roughness induced electronic Raman scattering. Surf. Sci. Lett. 92, L55–L57.
Park, J.-W., Shumaker-Parry, J.S., 2014. Structural study of citrate layers on gold nanoparticles: role of intermolecular interactions in stabilizing nanoparticles. J. Am. Chem. Soc. 136, 1907–1921.
Pei, L., Mori, K., Adachi, M., 2004. Formation process of two-dimensional networked gold nanowires by citrate reduction of $AuCl_4^-$ and the shape stabilization. Langmuir 20, 7837–7843.
Piella, J., Bastús, N.G., Puntes, V., 2016. Size-controlled synthesis of sub-10 nm citrate-stabilized gold nanoparticles and related optical properties. Chem. Mater. 28, 1066–1075.
Polte, J., 2015. Fundamental growth principles of colloidal metal nanoparticles–a new perspective. CrystEngComm 17, 6809–6830.
Polte, J., Ahner, T.T., Delissen, F., Sokolov, S., Emmerling, F., Thünemann, A.F., Kraehnert, R., 2010. Mechanism of gold nanoparticle formation in the classical citrate synthesis method derived from coupled in situ XANES and SAXS evaluation. J. Am. Chem. Soc. 132, 1296–1301.
Pong, B.-K., Elim, H.I., Chong, J.-X., Ji, W., Trout, B.L., Lee, J.-Y., 2007. New insights on the nanoparticle growth mechanism in the citrate reduction of gold(III) salt: formation of the Au nanowire intermediate and its nonlinear optical properties. J. Phys. Chem. C 111, 6281–6287.
Rodríguez-González, B., Mulvaney, P., Liz-Marzán, L.M., 2007. An electrochemical model for gold colloid formation via citrate reduction. Zeitschrift für Physikalische Chemie 221, 415–426.
Schwer, C., Kenndler, E., 1991. Electrophoresis in fused-silica capillaries: the influence of organic solvents on the electroosmotic velocity and the zeta potential. Anal. Chem. 63, 1801–1807.
Shahbazali, E., Hessel, V., Noël, T., Wang, Q., 2014. Metallic nanoparticles made in flow and their catalytic applications in organic synthesis. Nanotechnology Reviews 3, 65–86.
Singh, A., Shirolkar, M., Lalla, N.P., Malek, C.K., Kulkarni, S., 2009. Room temperature, water-based, microreactor synthesis of gold and silver nanoparticles. Int. J. Nanotechnol. 6, 541–551.
Slot, J.W., Geuze, H.J., 1985. A new method of preparing gold probes for multiple-labeling cytochemistry. Eur. J. Cell Biol. 38, 87–93.
Su, C.-H., Wu, P.-L., Yeh, C.-S., 2003. Sonochemical synthesis of well-dispersed gold nanoparticles at the ice temperature. J. Phys. Chem. B 107, 14240–14243.
Sugano, K., Uchida, Y., Ichihashi, O., Yamada, H., Tsuchiya, T., Tabata, O., 2010. Mixing speed-controlled gold nanoparticle synthesis with pulsed mixing microfluidic system. Microfluidics Nanofluidics 9, 1165–1174.
Tognalli, N.G., Cortés, E., Hernández-Nieves, A.D., Carro, P., Usaj, G., Balseiro, C.A., Vela, M.E., Salvarezza, R.C., Fainstein, A., 2011. From single to multiple Ag-layer modification of Au nanocavity substrates: a tunable probe of the chemical surface-enhanced Raman scattering mechanism. ACS Nano 5, 5433–5443.
Turkevich, J., Stevenson, P.C., Hillier, J., 1951. A study of the nucleation and growth processes in the synthesis of colloidal gold. Discuss. Faraday Soc. 11, 55–75.
Turkevich, J., Stevenson, P.C., Hillier, J., 1953. The formation of colloidal gold. J. Phys. Chem. 57, 670–673.
Wagner, J., Köhler, J.M., 2005. Continuous synthesis of gold nanoparticles in a microreactor. Nano Lett. 5, 685–691.
Werner, C., König, U., Augsburg, A., Arnhold, C., Körber, H., Zimmermann, R., Jacobasch, H.J., 1999. Electrokinetic surface characterization of biomedical polymers – a survey. Colloids Surf. A 159, 519–529.
Wuithschick, M., Birnbaum, A., Witte, S., Sztucki, M., Vainio, U., Pinna, N., Rademann, K., Emmerling, F., Kraehnert, R., Polte, J., 2015. Turkevich in new robes: key questions answered for the most common gold nanoparticle synthesis. ACS Nano 9, 7052–7071.
Xia, H., Bai, S., Hartmann, J., Wang, D., 2009. Synthesis of monodisperse quasi-spherical gold nanoparticles in water via silver(I)-assisted citrate reduction. Langmuir 26, 3585–3589.
Yang, S., Cheng, F., Yeh, C., Lee, G., 2010. Size-controlled synthesis of gold nanoparticles using a micro-mixing system. Microfluidics Nanofluidics 8, 303–311.
Yang, S., Wang, Y., Wang, Q., Zhang, R., Ding, B., 2007. UV irradiation induced formation of Au nanoparticles at room temperature: the case of pH values. Colloids Surf. A 301, 174–183.
Zhang, J., Wang, K., Teixeira, A.R., Jensen, K.F., Luo, G., 2017. Design and scaling up of microchemical systems: a review. Ann. Rev. Chem. Biomol. Eng. 8, 285–305.
Zhang, X.-Y., Hu, A., Zhang, T., Lei, W., Xue, X.-J., Zhou, Y., Duley, W.W., 2011. Self-assembly of large-scale and ultrathin silver nanoplate films with tunable plasmon resonance properties. ACS Nano 5, 9082–9092.